Received: 12 July 2022 | Revised: 28 April 2023 | Accepted: 16 May 2023

DOI: 10.1111/ter.12669

RESEARCH ARTICLE

Terra Nova WILEY

Burial in the western Central Andes through Oligocene to Miocene ignimbrite flare-ups recorded by low-temperature thermochronology in the Cañete Canyon, Peru

Laurence Audin[1] | Benjamin Gérard[1,2] | Cécile Gautheron[3] | Stéphane Schwartz[1] | Carlos Benavente[1,4] | Xavier Robert[1] | Peter van der Beek[5] | Rosella Pinna-Jamme[3] | Mélanie Balvay[1] | Matthias Bernet[1] | Audrey Margirier[6] | Swann Zerathe[1]

[1]Univ. Grenoble Alpes, IRD, ISTerre, Grenoble, France

[2]Laboratoire de Planétologie et Géosciences, CNRS UMR 6112, Nantes Université, Nantes, France

[3]Université Paris-Saclay, CNRS, GEOPS, Orsay, France

[4]Instituto Geológico, Minero y Metalúrgico INGEMMET, Lima, Peru

[5]Institut für Geowissenschaften, Universität Potsdam, Potsdam, Germany

[6]Institute of Earth Surface Dynamics, University of Lausanne, Lausanne, Switzerland

Correspondence
Laurence Audin, Univ. Grenoble Alpes, IRD, ISTerre, 38000 Grenoble, France.
Email: laurence.audin@ird.fr

Funding information
Agence Nationale de la Recherche, Grant/Award Number: ANR-12-NS06-0005-01; INGEMMET; Institut de Recherche pour le Développement; Labex OSUG, Grant/Award Number: ANR10 LABX56; INSU

Abstract

Thermochronological data are essential to constrain thermal and exhumation histories in active mountain ranges. In the Central Andes, bedrock outcrops are rare, being blanketed by widespread late Palaeogene–Neogene and younger volcanic formations. For this reason, the exhumation history of the Western Cordillera (WC) in the Peruvian Andes has only been investigated locally along the mountain range. Dense thermochronological data are only available in canyons of the Arequipa (16° S) and Cordillera Negra regions (10° S). We present new apatite (U-Th)/He and fission-track data from the 1 km deep Cañete Canyon (13° S), where the Oligo-Miocene deposits are preserved lying conformably on an Eocene palaeo-topographic surface. Thermal modelling of thermochronological data indicate that the 30–20 Ma ignimbrite deposits overlying the bedrock were thick enough to cause burial reheating. We demonstrate that burial associated with thick volcanic formations should be taken into account when interpreting thermochronological data from the WC or in similar volcanic-arc settings.

KEYWORDS
Cenozoic burial, Central Andes, flat slab subduction, thermochronology, Western Cordillera

1 | INTRODUCTION

The exhumation history of the Central Andes has been widely studied over the last decades to understand the climatic and tectonic drivers of orogenic evolution (e.g. Schildgen & Hoke, 2018; Sundell et al., 2019). Since the Cretaceous, the Western Cordillera (WC) in Peru experienced diachronous volcanic-arc activity and surface uplift (Soler & Bonhomme, 1990; Thouret et al., 2007). In southern Peru, the landscape is largely capped by km-thick Oligocene–Miocene ignimbrite deposits (Figures 1 and 2) and bedrock outcrops are rare (Mamani et al., 2010). To date, the thermal history of the WC has only been quantified along the main canyons of the Arequipa (16° S; Schildgen et al., 2009), Abancay (14° S; Ruiz et al., 2009) and Cordillera Negra (10° S; Margirier et al., 2015) regions. The timing and latitudinal variation of Miocene exhumation between these sites that are over 1000 km apart remain unconstrained, as does the

thermal impact of the major Oligocene–early Miocene ignimbrite flare-ups (Figure 1). To address these questions, we provide new apatite fission-track (AFT) and (U-Th)/He (AHe) data from an altitudinal profile located in bedrock below the ignimbrites in the upper part of the 1 km deep Cañete Canyon.

2 | GEOLOGICAL AND GEODYNAMIC SETTING

The WC in Chile and Peru constitutes the Pacific flank of the Andean Altiplano (Figure 1). It is characterized by a 4-km-high topographic step separating the Coastal Cordillera to the west and the discontinuous volcanic arc to the east (Mamani et al., 2010).

The WC is mainly composed of Precambrian gneiss and lower Palaeozoic granitic basement rocks, covered by Jurassic to Cretaceous volcanoclastic deposits (Tosdal et al., 1984). In the Cañete region, batholiths of the upper WC were emplaced at ~60–52 Ma (Figures 1 and 3; Noble et al., 2005). The Nazca flare-up produced a large volume of ignimbrites between 30 and 20 Ma, mapped from the Cañete to the Nazca Canyon (Figures 1 and 2; Tosdal et al., 1981). In Peru, 'ignimbrite' refers to voluminous (>1 km^3) pyroclastic deposits and explosive volcanism, exposing multiple flow units (Thouret et al., 2016; Wilson & Hildreth, 2003). These 'flare-ups' represent igneous production rates exceeding 25 $km^3\,Ma^{-1}\,km^{-1}$ (Brandmeier & Wörner, 2016). The ignimbrites covered the WC, filling preexisting canyons and capping the widespread Eocene erosion surface (Figure 1c; e.g. Freymuth et al., 2015; Marocco & de Muizon, 1988; Sébrier et al., 1988). In the forearc, this Eocene palaeo-topography is directly overlain by Cenozoic to Quaternary marine sediments (Figure 1; DeVries, 1998). It represents a remarkable marker that is incised, tilted and dipping towards the Pacific Ocean (Figure 2; Jeffery et al., 2013; Thouret et al., 2016; Wörner et al., 2002).

Along strike of the Peruvian Andes, changes in the dip of the subducting slab are argued to control volcanic activity and rock uplift in the Cordillera Negra region (Figure 1; 10° S; Margirier et al., 2015) and in the Ocoña–Colca region (16° S; Gunnell et al., 2010; Schildgen et al., 2007); no major thermal impact on the crust was recorded in either case (Margirier et al., 2016; Schildgen et al., 2009). In the Cañete region, slab flattening caused landward migration of volcanic activity during the Palaeogene (~50–30 Ma; Mamani et al., 2010). This time frame coincides with the initiation of counterclockwise oroclinal bending in the Central Andes (Roperch et al., 2011), leading to a stronger obliquity of convergence and partitioning of deformation in southern Peru with respect to northern Chile. Several studies combining structural geology and thermochronology suggested that this flat slab period is contemporaneous with rock uplift of the WC (e.g. Gérard et al., 2021; Noury et al., 2017). Following this phase, the slab steepened at ca. 30 Ma, triggering the ignimbrite flare-up in the Central Andes, before westward arc migration towards the present-day location at 15 Ma (Decou et al., 2011). Since the Miocene, low rates of exhumation and rock uplift have been proposed for the WC of Peru and Chile, based on low-temperature thermochronology, erosion (Gunnell et al., 2010; Schildgen et al., 2009; Van Zalinge et al., 2017) and tectonic studies (Benavente et al., 2017, 2021; Hall et al., 2012; Wörner et al., 2002).

Significance Statement

We provide apatite fission-track and AHe data along an altitudinal bedrock profile from the Cañete canyon in the western Andes of southern Peru. We demonstrate that it is essential (1) to use geological constraints in thermochronological models to take into account the exposure of the bedrock before Oligo-Miocene ignimbrite deposition and (2) to constrain a meaningful thermal history. Burial related to ignimbrite emplacement should be incorporated when interpreting thermochronological data in this area. Our new thermochronological data from the Cañete Canyon constrain the exhumation and the uplift history of the Western Cordillera on the Peruvian Pacific margin during the Oligo-Miocene Andean mountain building phase. This flat slab region (Nazca Plate subduction flattening initiated north of our site 15 Myr ago) corresponds to a transition area, and we document the evolution of the Cañete region since Oligocene–Miocene times, before Nazca Ridge arrival 4 Myr ago (addressed by Wipf et al., 2008). The significance of volcanic burial (by ignimbrites covering the bedrock and filling the early canyons) and its role in the thermal evolution of the upper crust has rarely been addressed before in a volcanic-arc setting. Numerous studies relying on thermochronological data to model exhumation or incision histories of the Andes do not consider this process. To our knowledge, only Colleps et al. (2021) applied apatite (U-Th)/He thermochronology to test the extent of the Deccan Traps on the Indian craton.

3 | SAMPLES AND METHODS

3.1 | Sample locations and sampling strategy

We collected six samples along a profile spanning ~2 km in elevation in the Cañete Canyon (Figures 1 and 2). The samples were selected from different igneous bedrock lithologies below the thick Miocene ignimbrite layers, between the valley bottom and the base of the ignimbrites (Figure 1; Table 1). We followed the approach of Schildgen et al. (2007, 2009) in representing the palaeo-elevation of the samples using their reconstructed depth beneath the base of the volcanic rocks (Table 1; Figure 4).

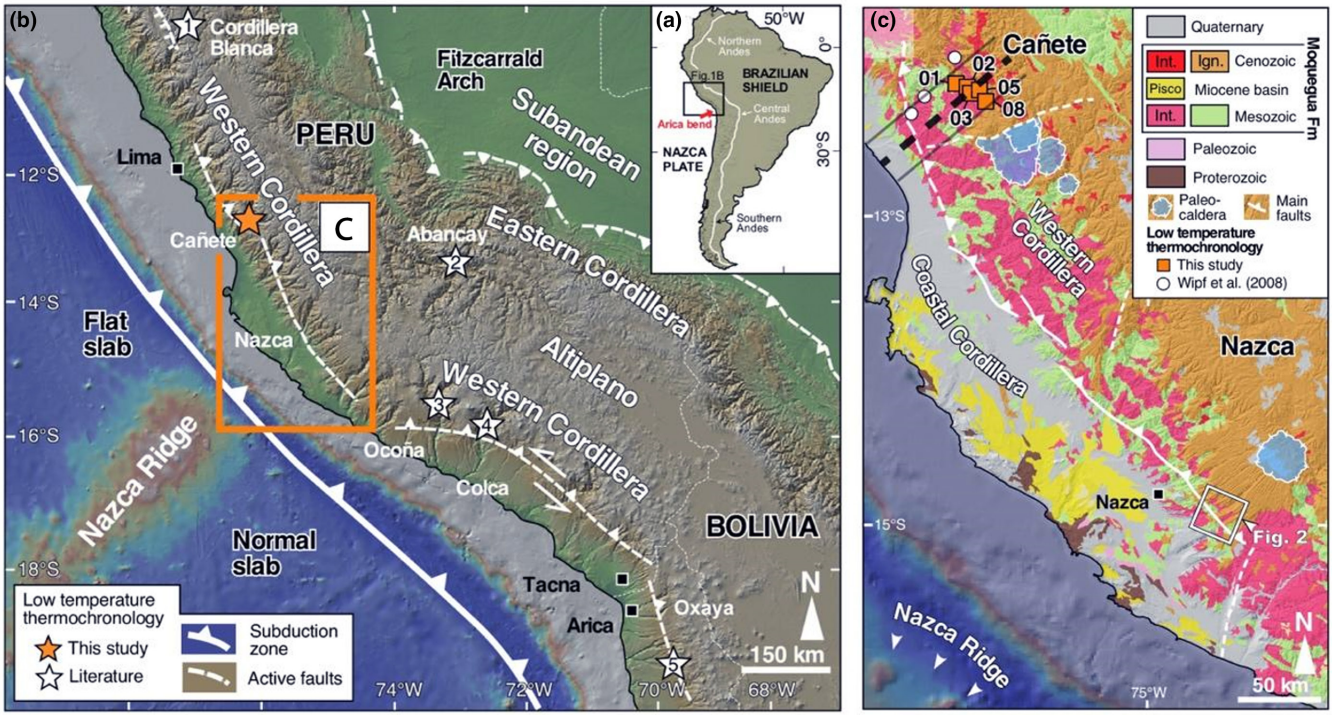

FIGURE 1 (a) Location of the study area in South America. The white line shows the extent of the Andes along the western flank of the continent. (b) Topographic map centred on the Peruvian Andes showing the location of the Western Cordillera, Altiplano, Eastern Cordillera and Subandean region. Location of the low-temperature thermochronological data from this study (orange star in Cañete) and from the literature [white stars; 1: Margirier et al. (2015); 2: Ruiz et al. (2009); Gérard et al. (2021); 3: Schildgen et al. (2009, 2010); 4: Gunnell et al. (2010)] and incision data [white star 5: Evenstar et al. (2020)] are marked on the map. (c) Geological map of the study area showing the Cañete sampling sites and Nazca Ignimbrite in the Western Cordillera. Simplified sample numbers from this study are also reported. The Moquegua formation includes Cenozoic intrusive (int.) and volcanic (ign.: ignimbrite) rocks, Miocene Pisco sediments and Mesozoic Cenozoic intrusive (int.) and volcanic rocks. Palaeozoic, Proterozoic and Quaternary rocks occur mainly along the Coastal Cordillera. Along the Western Cordillera, the Cenozoic Nazca ignimbrite unconformably covers the outcropping Mesozoic (intrusive and volcanics) and Cenozoic intrusive rocks. Positions of palaeo-calderas and main faults are indicated. The white square locates the aerial photo of Figure 2. The black outline comprising the Cañete Canyon data and the dashed black line shows the location of the swath profile of Figure 3.

3.2 | Thermal-history modelling

Thermal-history modelling was performed jointly for all the data with the QTQt code (Gallagher, 2012). The inversion code incorporates a radiation damage-dependent kinetic model for He diffusion (Flowers et al., 2009), as well as a multi-kinetic AFT annealing model (Ketcham et al., 2007). According to the oldest thermochronological record and independent geological constraints on the timing of batholith emplacement (~60 Ma), the time span explored starts at 60–52 Ma (Figure 5). We designed two models, both starting with an initial temporal and thermal constraint corresponding to pluton emplacement. The first model is free from any other constraints. In the second model, we constrained samples to be close to the surface at ~28 ± 2 Ma, based on the field evidence discussed above (Figure 5; Table 2 for parameter values). For both models, we did not impose any reheating event, but we allow the code to explore *T*–*t* paths that include reheating. To test the robustness of thermal histories, we compared predicted ages from the most likely *T*–*t* paths derived by QTQt to the observed data (Figure 5).

4 | RESULTS

4.1 | AFT and AHe data

Five and four samples were analysed for AHe and AFT respectively. Data from this study and from Wipf et al. (2008) are reported along a south-west–north-east profile (Figure 3) and as a function of palaeo-depth beneath the Oligocene–early Miocene ignimbrites (Figure 4 and Data S1). The spatial pattern of AFT and AHe ages forms a 'boomerang' shape, with the youngest AHe ages encountered ~60 km from the coast at the valley bottom (Figure 3). Two AFT ages, corresponding to the highest sample (3002 m) and to the lowest sample (295 m; Wipf et al., 2008), are similar to the crystallization age of the batholith (Figure 3). AFT ages of samples from the lower part of the profile (1019–2459 m) are the same within error (24.1 ± 5.5, 22.7 ± 3.7 and 20.9 ± 3.7 Ma) and are partially annealed, as confirmed by limited track-length data (Table 3). AHe ages are younger than the corresponding AFT ages, with corrected ages ranging from 1.8 ± 0.2 to 2.9 ± 0.3 Ma for the lowermost sample (1019 m) to similar ages of

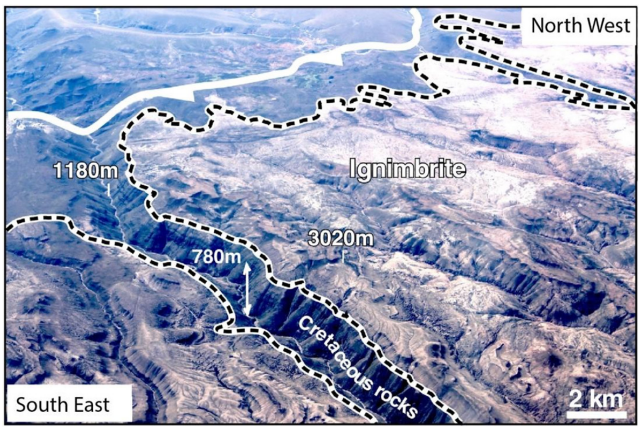

FIGURE 2 Aerial photograph close to the Western Cordillera front (white line) near the city of Nazca, showing the best-preserved ignimbrite deposits (extent outline by black dashed lines) in the Cañete-Nazca region. Maximum (3020 m asl) and minimum (1180 m asl) elevations are indicated. Deep canyons (>780 m), cutting through both Nazca ignimbrite and Cretaceous rocks, indicate an episode of incision after deposition of the ignimbrites.

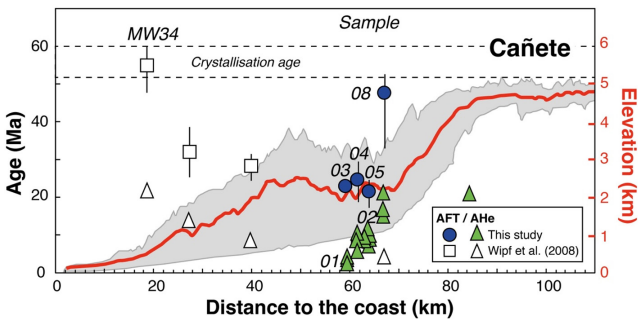

FIGURE 3 AFT and AHe ages as a function of distance to the coast, overlain on a topographic swath profile of the Cañete Canyon (refer to Figure 1c for location). Ar–Ar crystallisation ages of the plutonic rocks (Noble et al., 2005) are reported in Table 1. AFT, apatite fission-track.

7.8 ± 0.5, 7.1 ± 1.4 and 7.8 ± 1.7 Ma for the samples with elevations between 1485 and 2153 m (Table 4). The highest-elevation sample (08, 3002 m) shows a significantly older AHe age (13.8 ± 1.2 Ma). The apatite grains are characterized by low to moderate effective uranium contents (eU = U + 0.24 × Th), ranging from 2 to 38 ppm (Table 4), except for sample 12–04 (38–237 ppm).

4.2 | Thermal-history modelling

AHe and AFT ages predicted by QTQt reproduce the observed ages well for both thermal histories (Figure 5), with or without a *t–T* constraint related to the erosion surface at the base of the ignimbrite.

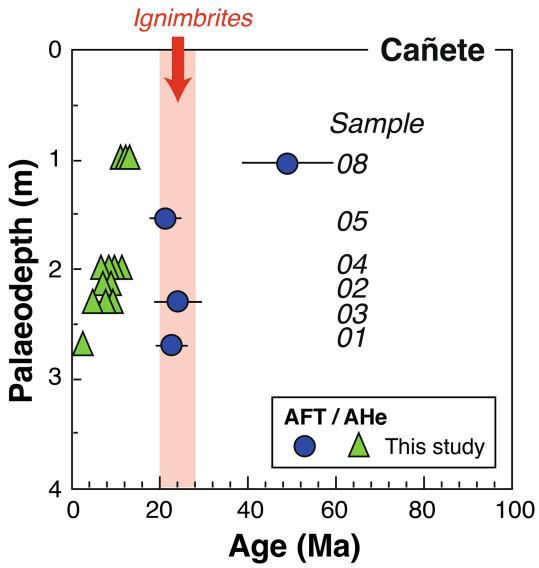

FIGURE 4 AFT and AHe ages as a function of palaeo-depth below the ignimbrite for the Cañete profile samples. The AFT age of sample 08 reflects post-crystallization and pre-ignimbrite cooling of the bedrock. The AHe age of sample 08 was reset by burial heating below the ignimbrites but not its AFT age. The AHe age reflects post-ignimbrite exhumation cooling from about 15 Ma. AFT, apatite fission-track.

TABLE 1 Samples location and description.

Sample	Lat (°S)	Long (°W)	Alt. (m)	Palaeo depth (m)	Distance to the coast (km)	Rock type	AHe	AFT
01	12.8541	75.9412	1019	2700	60	Coarse granodiorite	X	X
02	12.8720	75.8908	1485	2150	63	Granite	X	
03	12.8816	75.8645	1874	2300	62	Coarse granodiorite	X	X
04	12.8906	75.8579	2153	2000	64	Granodiorite	X	
05	12.8972	75.8559	2458	1550	64	Granodiorite		X
08	12.9350	75.7915	3002	1000	67	Porphyritic rhyolite	X	X

Note: For all samples, a crystallization age of 60–52 Ma is assumed (Noble et al., 2005).
Abbreviation: AFT, apatite fission-track.

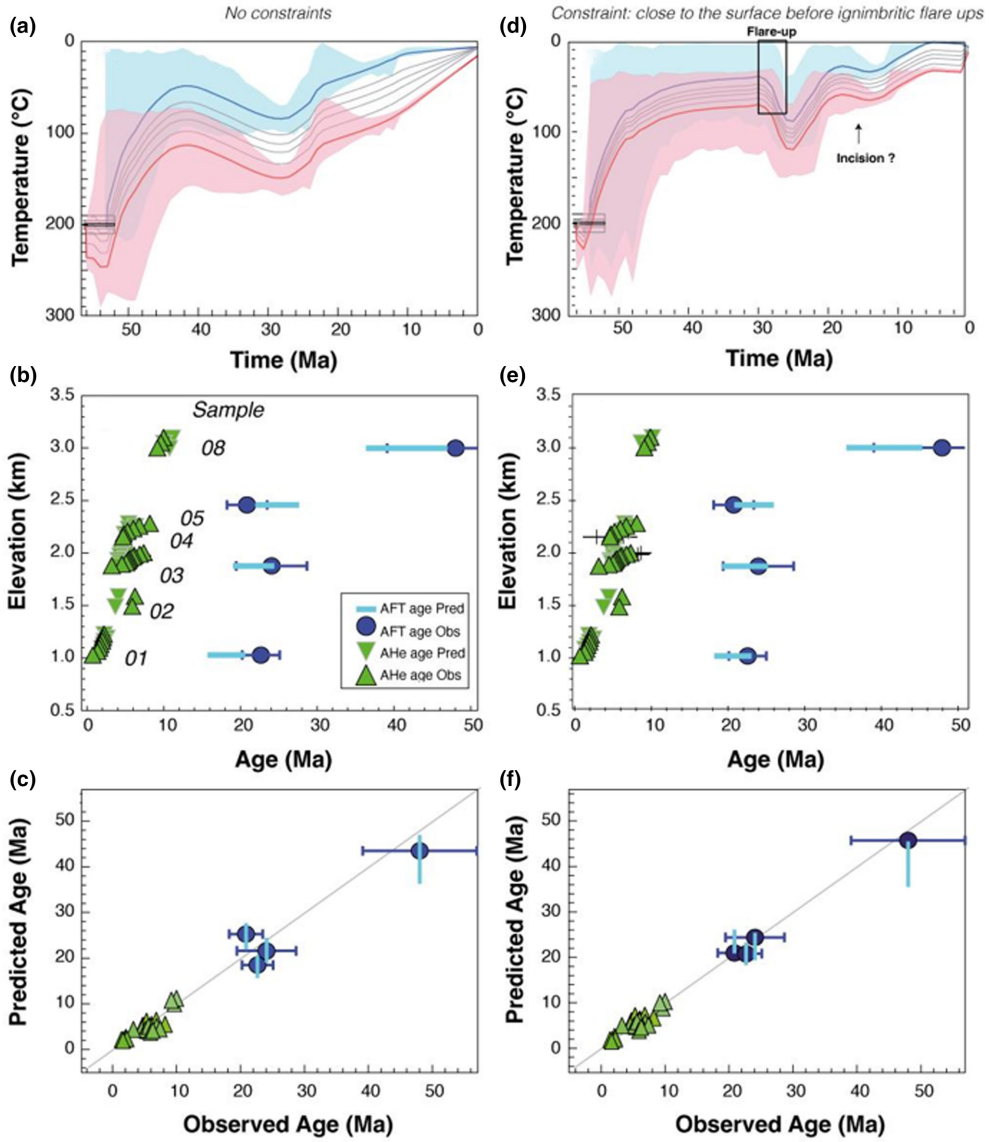

FIGURE 5 Time–temperature (*T–t*) modelling results for the Cañete Canyon profile using QTQt modelling, predicted (Pred) and observed (Obs) AFT and AHe ages. (a) *T–t* history modelled without additional constraints; associated predicted ages are shown in (b) (age – elevation plot) and (c) (predicted vs. observed age). (d) *T–t* history modelled with geological constraint (samples close to the surface at 30–26 Ma); associated predicted ages are shown in (e) (age–elevation plot) and (f) (predicted vs. observed age). Green boxes in (a) and (d) correspond to the pluton emplacement constraints (initial constraint in Table 4). Lines in (a) and (d) represent the best-fit *T–t* model for each sample of the profile, with the red and blue lines corresponding to the lowest and highest sample respectively. Red and blue shaded areas represent the uncertainty envelopes of the best-fit models for the lowest and highest sample respectively. The vertical light blue bars in (b, c, e, f) represent the mean 95% credible range for the predictions from all thermal-history models. In some cases, the best model age prediction is out of the 95% credible range. AFT, apatite fission-track.

Both thermal histories indicate an initial cooling episode from ~55 to ~40 Ma, constrained by the crystallization age and the oldest AFT age of the profile (Figure 5a–d), but the later thermal histories differ. The thermal history without constraint indicates reheating from ~40 to ~30 Ma followed by renewed cooling from ~30 Ma to the present-day. The thermal history with an additional *t–T* constraint (samples close to the surface at 28 ± 2 Ma) indicates slow cooling from ~40 to 30 Ma, followed by a short reheating phase from 30 to 25 Ma. Subsequently, the model indicates two cooling phases, a first one from 25 to 20 Ma and a second cooling phase starting at ~14 Ma. Both time–temperature histories require reheating of the Cañete samples at 30 Ma before final cooling, but the most recent part of the cooling history is significantly different for the two models (Figure 5).

5 | DISCUSSION

The difference between the two thermal histories indicates that it is essential to implement the *t–T* constraints related to the documented

Eocene–Oligocene palaeo-erosion surface in the WC (Figure 5d). The thermal history including this geological constraint reproduces the observed AHe and AFT data well (Figure 5e,f). We favour this model, as it explicitly includes the formation of the Eocene erosion surface and corresponding near-surface position of the rocks prior to ignimbrite eruption. Some AFT ages (samples 08 of this study and MW34 of Wipf et al., 2008; Figure 3) overlap with the crystallisation ages and both thermal models reveal that our samples experienced cooling during the Palaeocene–Eocene. We suggest that this initial cooling phase corresponds to post-magmatic cooling after Palaeocene intrusion (Figure 5).

Our preferred thermal history shows slow cooling from 45 to 30 Ma (Figure 5d–f), which we link to moderate erosion and development of the extensive erosion surface prior to 30 Ma (Noble et al., 1979) on which ignimbrites were deposited in the region between Cañete and Arequipa (Noble et al., 2005). This model is consistent with previous studies showing the WC to be eroded to a low-altitude topography in a semi-arid context, unroofing the plutonic complexes (Margirier et al., 2015; Quang et al., 2005).

Thermochronological data and modelling indicate that burial related to ignimbrite deposition during volcanic flare-ups impacted the thermal history of the Cañete bedrock samples (Figure 5). Both our models show reheating, which reaches a peak at ~30–25 Ma, synchronous with the timing of thick ignimbrite deposition (Figure 5a,d). These major igneous episodes may also have contributed to an increase in the local geothermal gradient at that time. However, such an increase in the geothermal gradient is not recorded in the regional data (Gérard et al., 2021; Schildgen et al., 2009). We suggest that heating was related to burial caused by the emplacement of a large volume of volcanic deposits rather than magmatic heating, because the AFT age of the highest-elevation sample (08) is not reset. For a geothermal gradient between 30 and 40°C/km (Springer & Förster, 1998), the recorded ~50°C heating would correspond to an ignimbrite thickness between 1.7 and 1.3 km. Whereas the model without constraint suggests continuous final cooling since 25 Ma, the model including a surface constraint shows a two-stage cooling history, with final cooling starting at ~14 Ma (Figure 5d) that we related to major canyon incision, as observed southwards in the Ocoña and Colca Canyons (Gunnell et al., 2010; Schildgen et al., 2007, 2009; Thouret et al., 2016).

We propose a palaeo-geographic model for the evolution of the WC, summarizing the geodynamic implications of our data integrated into previous regional models of exhumation (Figure 6). Geochronological and thermochronological data indicate intrusion emplacement and post-magmatic cooling during the Palaeocene (Figure 6a) followed by erosion of the WC forming an extensive Eocene erosional surface. Previous studies proposed regional rock uplift to occur from 50 to 14 Ma, less than 300 km from our study area south in the WC (Evenstar et al., 2020) and east in the Altiplano (Gérard et al., 2021). Rock uplift resumed at ca. 30–20 Ma in both Cordilleras and in the Altiplano (e.g. Sundell et al., 2019). Before ~30 Ma, the topography was at 1–2 km above the sea level, developing a low-relief plateau, which was subsequently capped by the extensive regional ignimbrites between ~30 and 20 Ma (Figure 6b; Thouret et al., 2016). In this region of the Central Andes, δ^2H stable isotopic analyses of volcanic glass yield an elevation of ~2 km at ~20 Ma (Sundell et al., 2019). The present-day elevation of up to 3 km was only reached at ~15 Ma (Figure 6c), similar to inferred topographic histories in southern Peru (Ocoña–Colca region; Roperch

TABLE 2 Inversion parameters for QTQt modelling.

Thermochronological data	
Samples and data used	AFT and AHe from this study
Data treatment	
AHe data (Rs, U, Th, He content)	Kinetic: Flowers et al. (2009)
AFT data and tracks length	Kinetic: Ketcham et al. (2007)
Additional geological information and constraints	
Present-day temperature	20°C
Initial constraint	54 ± 2 Ma to 200 ± 10°C
Simulation 'no constraints'	No additional constraints
Simulation 'constraint: close to the surface before ignimbrites deposition'	28 ± 2 Ma to 40 ± 40°C
Number of iterations in QTQt	Pre: 100,000, post: 100,000

Abbreviation: AFT, apatite fission-track.

TABLE 3 Apatite fission-track (AFT) data.

Sample	Grains No.	Ns	Ni	Nd	ρs $\times10^5$ (tracks/cm^2)	ρi	ρd	*U* ppm	Central ages ±2σ (Ma)	$P\chi^2$ %	Number of confined tracks	Mean track length (μm)	Dpar ± 2σ (μm)
01[a]	21	444	2499	4099	3.56	20.10	10.34	29	22.7 ± 3.7	1.0	3	12.2	1.4 ± 0.4
03[a]	18	134	711	4104	1.58	8.4	10.35	12	24.1 ± 5.5	3.3	-	-	
05[a]	20	317	1941	4108	4.89	29.90	10.35	43	20.9 ± 3.7	0.7	3	13.0	-
08	20	218	484	4115	2.27	5.05	11.99	6	48.0 ± 10.8	14.7	-	-	-

Note: Fission tracks were counted by M. Balvay at ISterre GTC using a zeta value of 247.2 ± 16.1. The uncertainty of the AFT ages is given as a 2σ range.

[a]Not covered by ignimbrite.

TABLE 4 Apatite (U-Th)/He data; AHe ages are corrected from alpha ejection using the F_T factor (Ketcham et al., 2011).

ID	Name	Weight (μg)	F_T	Rs (μm)	^{4}He (nccSTP/g)	U (ppm)	Th (ppm)	Sm (ppm)	eU (ppm)	Th/U	Age (Ma)	Age c[a] (Ma)
1975	01-RPA	3.2	0.79	55	9100	27	40	471	36	1.5	2.1	2.6±0.2
1979	01-RPB	5.1	0.80	62	9444	26	45	245	37	1.7	2.1	2.6±0.2
1981	01-RPC	3.1	0.80	51	7000	31	39	318	40	1.3	1.4	1.8±0.2
1985	01-RPE	2.9	0.77	52	3871	13	19	190	18	1.4	1.8	2.3±0.2
1987	01-RPF	2.8	0.77	52	10,764	28	47	443	40	1.7	2.2	2.9±0.3
1993	01-RPG	1.9	0.73	45	7264	26	42	331	36	1.6	1.6	2.2±0.2
1995	02-RPA	3.4	0.79	56	33,451	36	42	465	46	1.1	5.9	7.5±0.7
1997	02-RPB	6.2	0.79	65	27,291	26	40	283	35	1.6	6.4	8.1±0.7
2295	03-RPA	4.9	0.81	58	12,773	8	29	338	15	3.7	7.1	8.8±0.8
2008	03-RPB	5.3	0.78	65	12,815	10	28	331	17	2.7	6.0	7.7±0.7
2010	03-RPC	3.2	0.78	54	11,138	10	40	457	19	4.2	4.7	6.0±0.5
2012	03-RPD	4.5	0.81	62	23,976	18	61	401	33	3.4	6.0	7.4±0.7
2016	03-RPE	2.5	0.75	50	17,308	13	53	497	26	4.1	5.5	7.3±0.7
2018	03-RPF	2.9	0.78	53	9591	8	27	419	15	3.3	5.2	6.7±0.6
2020	03-RPG	3.1	0.77	53	11,437	10	33	450	17	3.4	5.3	6.8±0.6
2022	03-RPH	6.2	0.81	66	9036	7	25	293	13	3.7	5.7	7.0±0.6
2024	03-RPI	3.4	0.77	53	7284	10	33	458	18	3.2	3.2	4.2±0.4
2028	03-RPL	3.5	0.78	55	17,824	11	35	423	20	3.0	7.3	9.4±0.8
2030	04-RPB	1.9	0.74	49	38,709	56	45	666	67	0.8	4.7	6.4±0.6
2032	04-RPC	3.5	0.77	45	265,701	208	246	581	267	1.2	8.2	10.6±1.0
2034	04-RPD	3.1	0.80	55	28,823	33	24	404	38	0.8	6.1	7.7±0.7
2036	04-RPA	2.2	0.76	48	40,379	59	40	543	69	0.7	4.8	6.3±0.6
2040	04-RPE	4.2	0.76	56	150,271	138	181	450	181	1.3	6.9	9.1±0.8
2042	04-RPF	2.9	0.78	53	153,045	166	297	693	237	1.8	5.3	6.9±0.6
54	08-RPA	1.86	0.71	48.2	29,298	12.8	49.7	174	24.8	3.9	9.8	13.8±1.2
62	08-RPB	4.05	0.76	58.6	19,596	8.4	33.5	103	16.5	4.0	9.8	12.9±1.1
71	08-RPC	4.45	0.80	58.3	13,143	5.5	24.0	91	11.4	4.3	9.6	12.0±1.0

Note: 'F_T' geometric correction factor (Ketcham et al., 2011). 'Rs' is the equivalent-sphere radius calculated using the procedure of Gautheron and Tassan-Got (2010). 'Age c' is the age corrected by the crystal geometry and ejection factor F_T. The 1σ error of the AHe age is considered at 8%, reflecting the sum of errors in the ejection factor correction and age dispersion of the standards.

[a]Corrected, AHe age from alpha ejection using the F_T factor (from Ketcham et al., 2009).

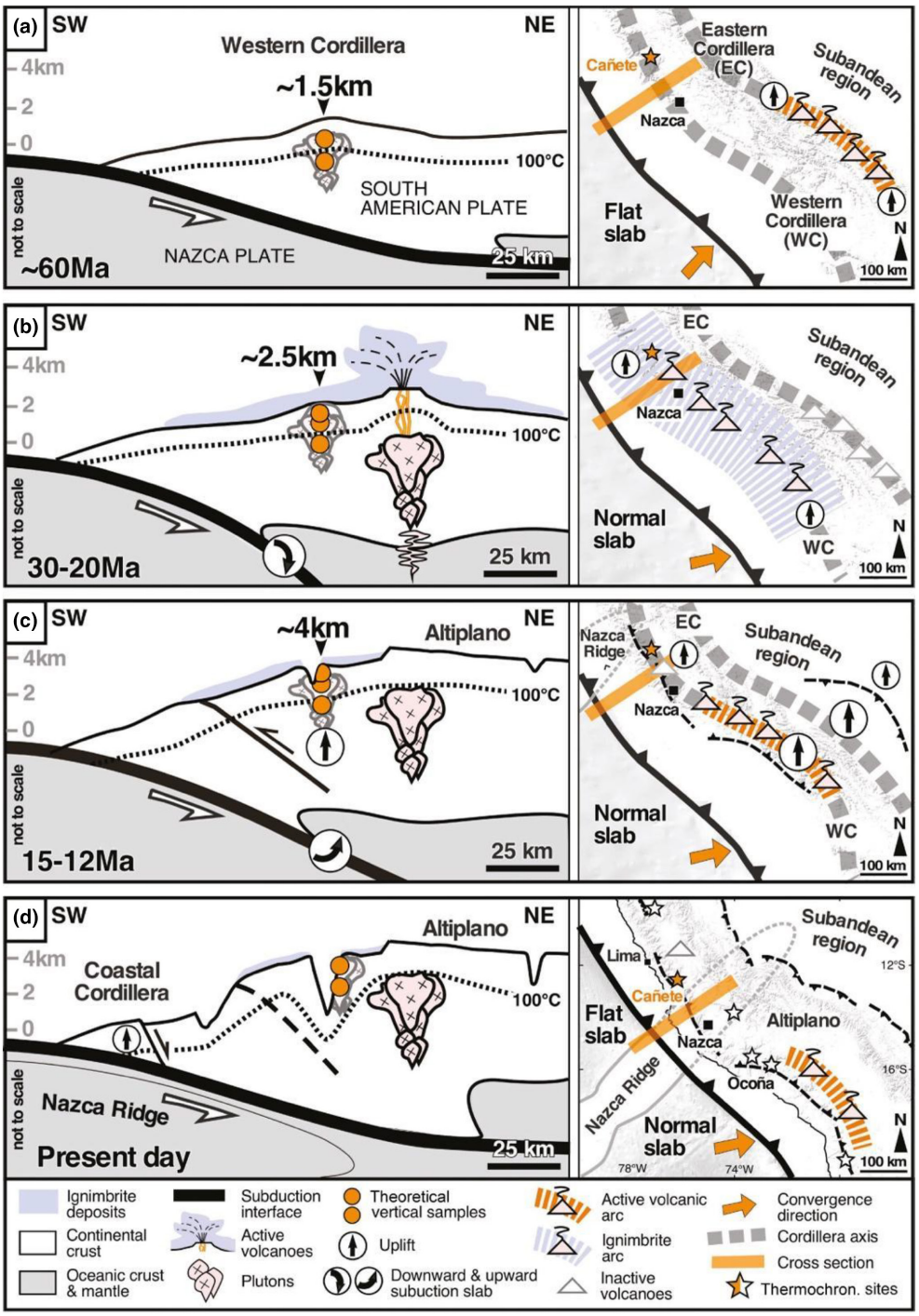

FIGURE 6 Schematic models of the topographic and volcanic evolution of the Western Cordillera at 60 Ma, 30–20 Ma, 15–12 Ma and the present day. The orange line on the maps shows the location of the corresponding schematic cross-section.

et al., 2011; Schildgen et al., 2009) or Chile (18° S to 22° S; Van Zalinge et al., 2017).

The western margin of the Andes has been undergoing uplift since the early Miocene (Evenstar et al., 2020) or even earlier since the Oligocene (Barnes & Ehlers, 2009; Van Zalinge et al., 2017). Jeffery et al. (2013) argued that the evolution of the Ocoña Canyon is consistent with local plateau elevations of 1–3 km at 16 Ma and either steady or punctuated uplift of 1.5–3.5 km since. The uplift of this region from Peru to Chile is accommodated by reverse fault systems (Figure 1; Benavente et al., 2021; Victor et al., 2004) accompanied by regional monoclinal tilting (Schildgen et al., 2009; Van Zalinge et al., 2017). There are no marked changes in regional tectonic uplift from North to South.

Valley incision was a long-term response to plateau uplift and initiated after 15 Ma in Peru (Schildgen et al., 2009), after monoclinal

deformation (from Nazca, Tacna in Peru to Oxaya in Chile; Figure 1) and oroclinal bending of the WC, as observed by palaeomagnetic data in southern Peru (Roperch et al., 2011). At ~8 Ma, the WC experienced a shift to more humid climatic conditions, with the development of large fluvial systems producing re-incision or development of erosional surfaces in the forearc (Figure 6d; Evenstar et al., 2020).

6 | CONCLUSION

Thermal modelling of our low-temperature thermochronology data, together with geological data, demonstrates the influence of the Oligocene–early Miocene ignimbrite flare-up on the thermochronological record in the Western Central Andes. This study provides new constraints on landscape and relief evolution since ~55 Ma in the WC of southern Peru. Our results are compatible with previous data suggesting slow Palaeogene exhumation to the east in the Altiplano, but highlight this pattern in the forearc at this latitude for the first time. Additionally, they also demonstrate that slow exhumation of the WC extended latitudinally from 10° S to 17° S along the Western Andes in Peru, apparently independent of Nazca Ridge migration. Finally, the post-15 Ma exhumation of the WC in the Central Andes is captured in thermochronological records spanning the forearc from southern Peru to northern Chile. This tectonic episode induced major incision of canyons despite regionally contemporaneous low denudation rates in the forearc.

ACKNOWLEDGEMENTS

This study was supported by the Institut de Recherche pour le Développement, France, and co-funded by the INGEMMET in Peru. We thank F. Delgado for assistance in the field, and F. Coeur and F. Senebier for sample processing. L. Bordier is thanked for help during U and Th measurements and E. Douville for access to the ICP-QMS. The analytical part of the project was funded by INSU and ANR (ANR-12-NS06-0005-01 HeDiff project). ISTerre is part of Labex OSUG@2020 (ANR10 LABX56).

DATA AVAILABILITY STATEMENT

The data that support the findings of this study are available from the corresponding author upon reasonable request.

ORCID

Laurence Audin https://orcid.org/0000-0002-4510-479X
Benjamin Gérard https://orcid.org/0000-0001-8143-8343
Matthias Bernet https://orcid.org/0000-0001-5046-7520

REFERENCES

Barnes, J. B., & Ehlers, T. A. (2009). End member models for Andean Plateau uplift. *Earth-Science Reviews*, *97*, 105–132. https://doi.org/10.1016/j.earscirev.2009.08.003

Benavente, C., Wimpenny, S., Rosell, L., Robert, X., Palomino, A., & Audin, L. (2021). Paleoseismic evidence of an Mw 7 pre-Hispanic earthquake in the Peruvian forearc. *Tectonics*, *40*, e2020TC006479.

Benavente, C., Zerathe, S., Audin, L., Hall, S. R., Robert, X., Delgado, F., & ASTER Team. (2017). Active transpressional tectonics in the Andean forearc of southern Peru quantified by ^{10}Be surface exposure dating of an active fault scarp. *Tectonics*, *36*, 1662–1678.

Brandmeier, M., & Wörner, G. (2016). Compositional variations of ignimbrite magmas in the Central Andes over the past 26 Ma—A multivariate statistical perspective. *Lithos*, *262*(1), 713–728.

Colleps, C. L., McKenzie, N. R., Guenthner, W. R., Sharma, M., Gibson, T. M., & Stockli, D. F. (2021). Apatite (U-Th)/He thermochronometric constraints on the northern extent of the Deccan large igneous province. *Earth and Planetary Science Letters*, *571*, 117087.

Decou, A., von Eynatten, H., Mamani, M., Sempere, T., & Wörner, G. (2011). Cenozoic forearc basin sediments in Southern Peru (15–18°S): Stratigraphic and heavy mineral constraints for Eocene to Miocene evolution of the Central Andes. *Sedimentary Geology*, *237*, 55–72.

DeVries, T. J. (1998). Oligocene deposition and Cenozoic sequence boundaries in the Pisco Basin (Peru). *Journal of South American Earth Sciences*, *11*, 217–231.

Evenstar, L. A., Mather, A. E., & Hartley, A. J. (2020). Using spatial patterns of fluvial incision to constrain continental-scale uplift in the Andes. *Global and Planetary Change*, *186*, 103119.

Flowers, R., Ketcham, R. A., Shuster, D., & Farley, K. A. (2009). Apatite (U-Th)/He thermochronology using a radiation damage accumulation and annealing model. *Geochimica et Cosmochimica Acta*, *73*, 2347–2365.

Freymuth, H., Brandmeier, M., & Wörner, G. (2015). The origin and crust/mantle mass balance of Central Andean ignimbrite magmatism constrained by oxygen and strontium isotopes and erupted volumes. *Contributions to Mineralogy and Petrology*, *169*, 1–24.

Gallagher, K. (2012). Transdimensional inverse thermal history modelling for quantitative thermochronology. *Journal of Geophysical Research*, *117*, B02408.

Gautheron, C., & Tassan-Got, L. (2010). A Monte Carlo approach to diffusion applied to noble gas/helium thermochronology. *Chemical Geology*, *273*, 212–224.

Gérard, B., Robert, X., Audin, L., Valla, P. G., Bernet, M., & Gautheron, C. (2021). Differential exhumation of the Eastern Cordillera in the Central Andes: Evidence for south-verging Backthrusting (Abancay Deflection, Peru). *Tectonics*, *40*, e2020TC006314.

Gunnell, Y., Thouret, J. C., & Brichau, S. (2010). Low-temperature thermochronology in the Peruvian Central Andes: Implications for long-term continental denudation, timing of plateau uplift, canyon incision and lithosphere dynamics. *Journal of the Geological Society of London*, *167*, 803–815.

Hall, S. R., Farber, D. L., Audin, L., & Finkel, R. C. (2012). Recently active contractile deformation in the forearc of southern Peru. *Earth and Planetary Science Letters*, *337*, 85–92.

Jeffery, M. L., Ehlers, T. A., Yanites, B. J., & Poulsen, C. J. (2013). Quantifying the role of paleoclimate and Andean Plateau uplift on river incision. *Journal of Geophysical Research - Earth Surface*, *118*, 852–871.

Ketcham, R. A., Carter, A., Donelick, R. A., Barbarand, J., & Hurford, A. J. (2007). Improved modeling of fission-track annealing in apatite. *American Mineralogist*, *92*, 799–810.

Ketcham, R. A., Donelick, R. A., Balestrieri, M. L., & Zattin, M. (2009). Reproducibility of apatite fission-track length data and thermal history reconstruction. *Earth and Planetary Science Letters*, *284*, 3–4.

Ketcham, R. A., Gautheron, C., & Tassan-Got, L. (2011). Accounting for long alpha-particle stopping distances in (U–Th–Sm)/He geochronology: Refinement of the baseline case. *Geochimica et Cosmochimica Acta*, *75*, 7779–7791.

Mamani, M., Wörner, G., & Sempere, T. (2010). Geochemical variations in igneous rocks of the Central Andean orocline (13 S to 18 S): Tracing

crustal thickening and magma generation through time and space. *Geological Society of America Bulletin*, *122*, 162–182.
Margirier, A., Audin, L., Robert, X., Herman, F., Ganne, J., & Schwartz, S. (2016). Time and mode of exhumation of the Cordillera Blanca batholith (Peruvian Andes). *Journal of Geophysical Research: Solid Earth*, *121*, 6235–6249.
Margirier, A., Robert, X., Audin, L., Gautheron, C., Bernet, M., Hall, S., & Simon-Labric, T. (2015). Slab flattening, magmatism and surface uplift in the Cordillera Occidental (northern Peru). *Geology*, *43*, 1031–1034.
Marocco, R., & de Muizon, C. (1988). Le bassin Pisco, bassin Cénozoique d'avant-arc de la côte du Pérou central: analyse géodynamique de son remplissage. *Géodynamique*, *3*, 3–19.
Noble, D., Vidal, C., Angeles, C., Wise, J., Zanneti, K., & Spell, T. (2005). Caldera related ash-flow tuff of Paleocene age in central Perú and its significance for late Cretaceous and Paleocene magmatism, sedimentation and tectonism. *Sociedad Geológica del Perú*, *6*, 127–140.
Noble, D. C., Farrar, E., & Cobbing, E. J. (1979). The Nazca Group of south-central Peru: Age, source, and regional volcanic and tectonic significance. *Earth and Planetary Science Letters*, *45*, 80–86.
Noury, M., Philippon, M., Bernet, M., Paquette, J.-L., & Sempéré, T. (2017). Geological record of flat slab-induced extension in the southern Peruvian forearc. *Geology*, *45*, 723–726.
Quang, C. X., Clark, A. H., Lee, J. K. W., & Hawkes, N. (2005). Response of supergene processes to episodic Cenozoic uplift, pediment erosion, and ignimbrite eruption in the porphyry Copper Province of Southern Perú. *Economic Geology*, *100*, 87–114.
Roperch, P., Carlotto, V., Ruffet, G., & Fornari, M. (2011). Tectonic rotations and transcurrent deformation south of the Abancay deflection in the Andes of southern Peru. *Tectonics*, *30*, TC2010.
Ruiz, G. M. H., Carlotto, V., Van Heiningen, P. V., & Andriessen, P. A. M. (2009). Steady-state exhumation pattern in the Central Andes – SE Peru. *Special Publication. Geological Society of London*, *324*, 307–316.
Schildgen, T. F., Balco, G., & Shuster, G. L. (2010). Canyon incision and knickpoint propagation recorded by apatite (super 4) He/ (super 3) He thermochronometry. *Earth and Planetary Science Letters*, *293*(3–4), 377–387.
Schildgen, T. F., Hodges, K. V., Whipple, K. X., Pringle, M. S., van Soest, M., & Cornell, K. (2009). Late Cenozoic structural and tectonic development of the western margin of the central Andean Plateau in southwest Peru. *Tectonics*, *28*, TC4007.
Schildgen, T. F., Hodges, K. V., Whipple, K. X., Reiners, P. W., & Pringle, M. S. (2007). Uplift of the western margin of the Andean plateau revealed from canyon incision history, southern Peru. *Geology*, *35*, 523–526.
Schildgen, T. F., & Hoke, G. D. (2018). The topographic evolution of the Central Andes. *Elements*, *14*, 231–236.
Sébrier, M., Lavenu, A., Fornari, M., & Soulas, J. P. (1988). Tectonics and uplift in Central Andes (Peru, Bolivia and northern Chile) from Eocene to present. *Géodynamique*, *3*, 85–106.
Soler, P., & Bonhomme, M. G. (1990). Relation of magmatic activity to plate dynamics in central Peru from Late Cretaceous to present. *Geological Society of America Special Papers*, *241*, 173–192.
Springer, M., & Förster, A. (1998). Heat-flow density across the central Andean subduction zone. *Tectonophysics*, *291*, 123–139.
Sundell, K. E., Saylor, J. E., Lapen, T. J., & Horton, B. K. (2019). Implications of variable late Cenozoic surface uplift across the Peruvian central Andes. *Scientific Reports*, *9*, 4877.
Thouret, J. C., Jicha, B. R., & Paquette, J. L. (2016). A 25 Myr chronostratigraphy of ignimbrites in south Peru: Implications for the volcanic history of the Central Andes. *Journal of the Geological Society of London*, *173*, 734–756.
Thouret, J. C., Wörner, G., Gunnell, Y., & Singer, B. (2007). Geochronologic and stratigraphic constraints on canyon incision and Miocene uplift of the Central Andes in Peru. *Earth and Planetary Science Letters*, *263*, 151–166.
Tosdal, R. M., Clark, A. H., & Farrar, E. (1984). Cenozoic polyphase landscape and tectonic evolution of the Cordillera Occidental, southernmost Peru. *Geological Society of America Bulletin*, *95*, 1318–1332.
Tosdal, R. M., Farrar, E., & Clark, A. H. (1981). K-Ar geochronology of the late Cenozoic volcanic rocks of the Cordillera Occidental, southernmost Peru. *Journal of Volcanology and Geothermal Research*, *10*, 157–173.
Van Zalinge, M. E., Sparks, R. S. J., Evenstar, L. A., Cooper, F. J., & Aslin, J. (2017). Using ignimbrites to quantify structural relief growth and understand deformation processes: Implications for the development of the Western Andean Slope, northernmost Chile. *Lithosphere*, *9*(1), 29–45.
Victor, P., Oncken, O., & Glodny, J. (2004). Uplift of the western Altiplano plateau - Evidence from the Precordillera between 20° and 21°S (northern Chile). *Tectonics*, *23*, TC4004.
Wilson, C. J., & Hildreth, W. (2003). Assembling an ignimbrite: Mechanical and thermal building blocks in the Bishop Tuff, California. *The Journal of Geology*, *111*, 653–670.
Wipf, M., Zeilinger, G., Seward, D., & Schlunegger, F. (2008). Focused subaerial erosion during ridge subduction: Impact on the geomorphology in south-central Peru. *Terra Nova*, *20*, 1–10.
Wörner, G., Uhlig, D., Kohler, I., & Seyfried, H. (2002). Evolution of the West Andean Escarpment at 18°S (N. Chile) during the last 25 Ma: Uplift, erosion and collapse through time. *Tectonophysics*, *345*, 183–198.

SUPPORTING INFORMATION

Additional supporting information can be found online in the Supporting Information section at the end of this article.

Data S1.

How to cite this article: Audin, L., Gérard, B., Gautheron, C., Schwartz, S., Benavente, C., Robert, X., van der Beek, P., Pinna-Jamme, R., Balvay, M., Bernet, M., Margirier, A., & Zerathe, S. (2023). Burial in the western Central Andes through Oligocene to Miocene ignimbrite flare-ups recorded by low-temperature thermochronology in the Cañete Canyon, Peru. *Terra Nova*, *00*, 1–10. https://doi.org/10.1111/ter.12669